

High-Resolution Global Maps of 21st-Century Forest Cover Change

M. C. Hansen *et al.*

Science 342, 850 (2013);

DOI: 10.1126/science.1244693

This copy is for your personal, non-commercial use only.

If you wish to distribute this article to others, you can order high-quality copies for your colleagues, clients, or customers by [clicking here](#).

Permission to republish or repurpose articles or portions of articles can be obtained by following the guidelines [here](#).

The following resources related to this article are available online at www.sciencemag.org (this information is current as of November 19, 2013):

Updated information and services, including high-resolution figures, can be found in the online version of this article at:

<http://www.sciencemag.org/content/342/6160/850.full.html>

Supporting Online Material can be found at:

<http://www.sciencemag.org/content/suppl/2013/11/14/342.6160.850.DC1.html>

This article cites 32 articles, 10 of which can be accessed free:

<http://www.sciencemag.org/content/342/6160/850.full.html#ref-list-1>

16. T. Conrad, A. Akhtar, *Nat. Rev. Genet.* **13**, 123–134 (2011).
17. A. A. Alekseyenko et al., *Cell* **134**, 599–609 (2008).
18. A. A. Alekseyenko et al., *Genes Dev.* **27**, 853–858 (2013).
19. I. Marin, A. Franke, G. J. Bashaw, B. S. Baker, *Nature* **383**, 160–163 (1996).
20. Materials and methods are available as supplementary materials on *Science* Online.
21. Q. Zhou, C. E. Ellison, V. B. Kaiser, A. A. Alekseyenko, A. A. Gorchakov, D. Bachtrog, *PLoS Biol.* **11**, e1001711 (2013).
22. M. Steinemann, S. Steinemann, *Proc. Natl. Acad. Sci. U.S.A.* **89**, 7591–7595 (1992).
23. J. Jurka, *Rebase Reports* **12**, 1376 (2012).
24. V. V. Kapitonov, J. Jurka, *Trends Genet.* **23**, 521–529 (2007).
25. J. R. Bateman, A. M. Lee, C. T. Wu, *Genetics* **173**, 769–777 (2006).
26. Q. Zhou, D. Bachtrog, *Science* **337**, 341–345 (2012).
27. C. E. Grant, T. L. Bailey, W. S. Noble, *Bioinformatics* **27**, 1017–1018 (2011).

Acknowledgments: This work was funded by NIH grants (R01GM076007 and R01GM093182) and a Packard Fellowship to D.B. and a NIH postdoctoral fellowship to C.E.G. All DNA-sequencing reads generated in this study are deposited at the National Center for Biotechnology Information Short Reads Archive (www.ncbi.nlm.nih.gov/sra)

under the accession no. SRS402821. The genome assemblies are available at the National Center for Biotechnology Information under BioProject PRJNA77213. We thank Z. Walton and A. Gorchakov for technical assistance.

Supplementary Materials

www.sciencemag.org/content/342/6160/846/suppl/DC1

Materials and Methods

Supplementary Text

Figs. S1 to S20

Tables S1 to S3

References (28–54)

23 April 2013; accepted 30 September 2013

10.1126/science.1239552

High-Resolution Global Maps of 21st-Century Forest Cover Change

M. C. Hansen,^{1,*} P. V. Potapov,¹ R. Moore,² M. Hancher,² S. A. Turubanova,¹ A. Tyukavina,¹ D. Thau,² S. V. Stehman,³ S. J. Goetz,⁴ T. R. Loveland,⁵ A. Kommareddy,⁶ A. Egorov,⁶ L. Chini,¹ C. O. Justice,¹ J. R. G. Townshend¹

Quantification of global forest change has been lacking despite the recognized importance of forest ecosystem services. In this study, Earth observation satellite data were used to map global forest loss (2.3 million square kilometers) and gain (0.8 million square kilometers) from 2000 to 2012 at a spatial resolution of 30 meters. The tropics were the only climate domain to exhibit a trend, with forest loss increasing by 2101 square kilometers per year. Brazil's well-documented reduction in deforestation was offset by increasing forest loss in Indonesia, Malaysia, Paraguay, Bolivia, Zambia, Angola, and elsewhere. Intensive forestry practiced within subtropical forests resulted in the highest rates of forest change globally. Boreal forest loss due largely to fire and forestry was second to that in the tropics in absolute and proportional terms. These results depict a globally consistent and locally relevant record of forest change.

Changes in forest cover affect the delivery of important ecosystem services, including biodiversity richness, climate regulation, carbon storage, and water supplies (1). However, spatially and temporally detailed information on global-scale forest change does not exist; previous efforts have been either sample-based or employed coarse spatial resolution data (2–4). We mapped global tree cover extent, loss, and gain for the period from 2000 to 2012 at a spatial resolution of 30 m, with loss allocated annually. Our global analysis, based on Landsat data, improves on existing knowledge of global forest extent and change by (i) being spatially explicit; (ii) quantifying gross forest loss and gain; (iii) providing annual loss information and quantifying trends in forest loss; and (iv) being derived through an internally consistent approach that is exempt from the vagaries of different definitions, methods, and data inputs. Forest loss was defined as a stand-replacement disturbance or the com-

plete removal of tree cover canopy at the Landsat pixel scale. Forest gain was defined as the inverse of loss, or the establishment of tree canopy from a nonforest state. A total of 2.3 million km² of forest were lost due to disturbance over the study period and 0.8 million km² of new forest established. Of the total area of combined loss and gain (2.3 million km² + 0.8 million km²), 0.2 million km² of land experienced both loss and subsequent gain in forest cover during the study period. Global forest loss and gain were related to tree cover density for global climate domains, ecozones, and countries (refer to tables S1 to S3 for all data references and comparisons). Results are depicted in Fig. 1 and are viewable at full resolution at <http://earthenginepartners.appspot.com/science-2013-global-forest>.

The tropical domain experienced the greatest total forest loss and gain of the four climate domains (tropical, subtropical, temperate, and boreal), as well as the highest ratio of loss to gain (3.6 for >50% of tree cover), indicating the prevalence of deforestation dynamics. The tropics were the only domain to exhibit a statistically significant trend in annual forest loss, with an estimated increase in loss of 2101 km²/year. Tropical rainforest ecozones totaled 32% of global forest cover loss, nearly half of which occurred in South American rainforests. The tropical dry forests of South America had the highest rate of tropical forest loss, due to deforestation

dynamics in the Chaco woodlands of Argentina, Paraguay (Fig. 2A), and Bolivia. Eurasian rainforests (Fig. 2B) and dense tropical dry forests of Africa and Eurasia also had high rates of loss.

Recently reported reductions in Brazilian rainforest clearing over the past decade (5) were confirmed, as annual forest loss decreased on average 1318 km²/year. However, increased annual loss of Eurasian tropical rainforest (1392 km²/year), African tropical moist deciduous forest (536 km²/year), South American dry tropical forest (459 km²/year), and Eurasian tropical moist deciduous (221 km²/year) and dry (123 km²/year) forests more than offset the slowing of Brazilian deforestation. Of all countries globally, Brazil exhibited the largest decline in annual forest loss, with a high of over 40,000 km²/year in 2003 to 2004 and a low of under 20,000 km²/year in 2010 to 2011. Of all countries globally, Indonesia exhibited the largest increase in forest loss (1021 km²/year), with a low of under 10,000 km²/year from 2000 through 2003 and a high of over 20,000 km²/year in 2011 to 2012. The converging rates of forest disturbance of Indonesia and Brazil are shown in Fig. 3. Although the short-term decline of Brazilian deforestation is well documented, changing legal frameworks governing Brazilian forests could reverse this trend (6). The effectiveness of Indonesia's recently instituted moratorium on new licensing of concessions in primary natural forest and peatlands (7), initiated in 2011, is to be determined.

Subtropical forests experience extensive forestry land uses where forests are often treated as a crop and the presence of long-lived natural forests is comparatively rare (8). As a result, the highest proportional losses of forest cover and the lowest ratio of loss to gain (1.2 for >50% of tree cover) occurred in the subtropical climate domain. Aggregate forest change, or the proportion of total forest loss and gain relative to year-2000 forest area [(loss+gain)/2000 forest], equaled 16%, or more than 1% per year across all forests within the domain. Of the 10 subtropical humid and dry forest ecozones, 5 have aggregate forest change >20%, three >10%, and two >5%. North American subtropical forests of the southeastern United States are unique in terms of change dynamics because of short-cycle tree planting and harvesting (Fig. 2C). The disturbance rate of this ecozone was four times that of South American

¹Department of Geographical Sciences, University of Maryland, College Park, MD 20742, USA. ²Google, Mountain View, CA, USA. ³Department of Forest and Natural Resources Management, State University of New York, Syracuse, NY, USA. ⁴Woods Hole Research Center, 149 Woods Hole Road, Falmouth, MA 02540, USA. ⁵Earth Resources Observation and Science, United States Geological Survey, 47914 252nd Street, Sioux Falls, SD 57198, USA. ⁶Geographic Information Science Center of Excellence, South Dakota State University, Brookings, SD, USA.

*Corresponding author. E-mail: mhansen@umd.edu

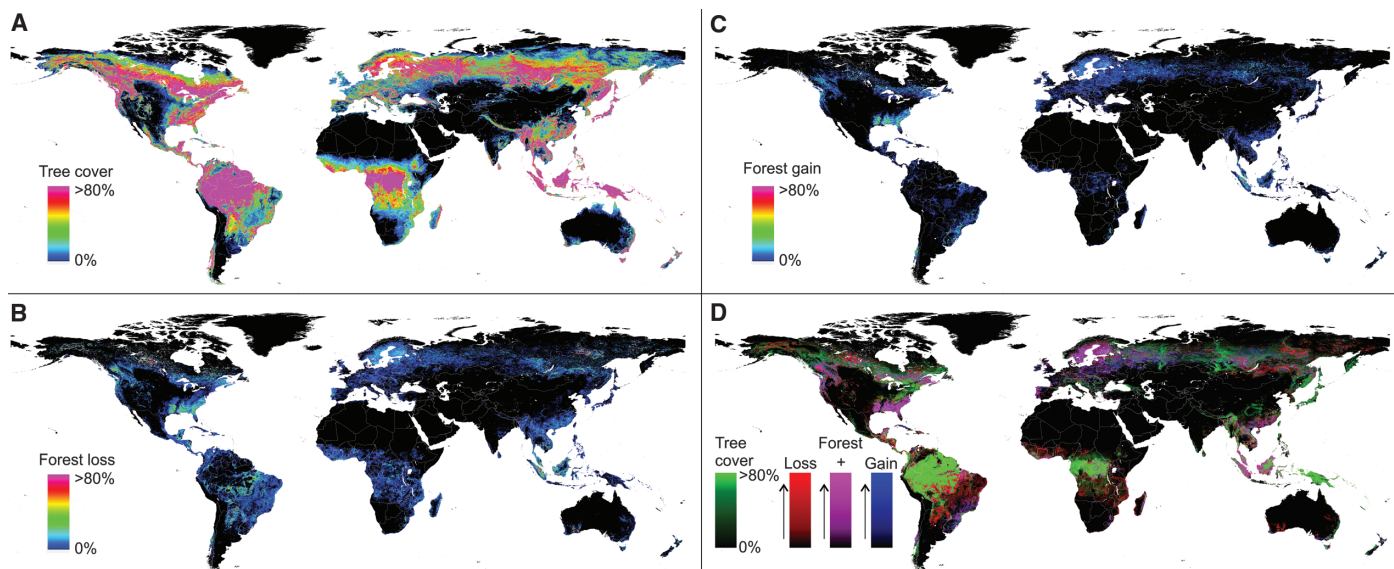


Fig. 1. (A) Tree cover, (B) forest loss, and (C) forest gain. A color composite of tree cover in green, forest loss in red, forest gain in blue, and forest loss and gain in magenta is shown in (D), with loss and gain en-

hanced for improved visualization. All map layers have been resampled for display purposes from the 30-m observation scale to a 0.05° geographic grid.

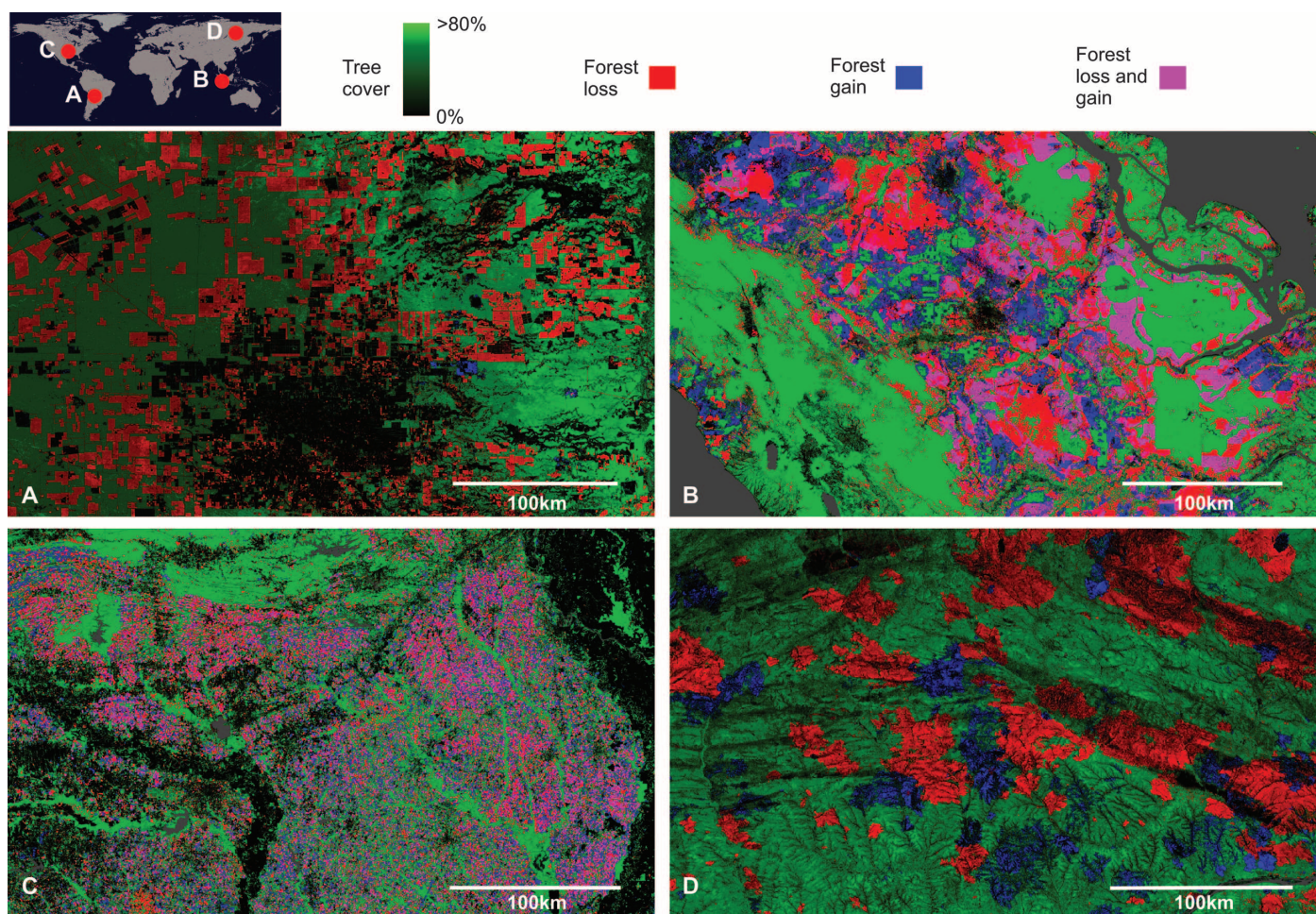


Fig. 2. Regional subsets of 2000 tree cover and 2000 to 2012 forest loss and gain. (A) Paraguay, centered at 21.9°S , 59.8°W ; (B) Indonesia, centered at 0.4°S , 101.5°E ; (C) the United States, centered at 33.8°N , 93.3°W ; and (D) Russia, centered at 62.1°N , 123.4°E .

rainforests during the study period; over 31% of its forest cover was either lost or regrown. Areas of colocated loss and gain (magenta tones in Fig. 1D), indicating intensive forestry practices, are found on all continents within the subtropical climate domain, including South Africa, central Chile, southeastern Brazil, Uruguay, southern China, Australia, and New Zealand.

The temperate climatic domain has a forestry-dominant change dynamic and a relatively low ratio of loss to gain (1.6 for >50% of tree cover). Oceanic ecozones, in particular, are similar to the subtropics in the intensity of indicated forest land use. The northwest United States is an area of intensive forestry, as is the entire range of temperate Canada. The intermountain West of North America exhibits a loss dynamic, largely due to fire, logging, and disease [for example, large-scale tree mortality due to mountain pine bark beetle infestation, most evident in British Columbia, Canada (9)]. Temperate Europe has a forestry dynamic with Estonia and Latvia exhibiting a high ratio of loss to gain. Portugal, which straddles the temperate and subtropical domains, has a complicated dynamic of forestry and forest loss due to fire; the resulting aggregate change dynamic is fourth in intensity globally. Elevated loss due to storm damage is indicated for a few areas. For example, a 2005 extratropical cyclone led to a historic blowdown of southern Sweden temperate forests, and a 2009 windstorm leveled extensive forest areas in southwestern France (10).

Fire is the most significant cause of forest loss in boreal forests (11), and it occurred across a range of tree canopy densities. Given slower regrowth dynamics, the ratio of boreal forest loss to gain is high over the study period (2.1 for >50% of tree cover). Boreal coniferous and mountain ecozones are similar in terms of forest loss rates, with North America having a higher overall rate

and Eurasia a higher absolute area of loss. Forest gain is substantial in the boreal zone, with Eurasian coniferous forests having the largest area of gain of all global ecozones during the study period, due to forestry, agricultural abandonment (12), and forest recovery after fire [as in European Russia and the Siberia region of Russia (Fig. 2D)]. Russia has the most forest loss globally. Co-located gain and loss are nearly absent in the high-latitude forests of the boreal domain, reflecting a slower regrowth dynamic in this climatic domain. Areas with loss and gain in close proximity, indicating forestry land uses, are found within nearly the entirety of Sweden and Finland, the boreal/temperate transition zone in eastern Canada, parts of European Russia, and along the Angara River in central Siberia, Russia.

A goal of large-area land cover mapping is to produce globally consistent characterizations that have local relevance and utility; that is, reliable information across scales. Figure S1 reflects this capability at the national scale. Two measures of change, (i) proportion of total aggregate forest change relative to year-2000 forest area [$(\text{loss} + \text{gain})/2000 \text{ forest}$], shown in column q of table S3; and (ii) proportion of total change that is loss [$\text{loss}/(\text{loss} + \text{gain})$], calculated from columns b and c in table S3, are displayed. The proportion of total aggregate forest change emphasizes countries with likely forestry practices by including both loss and gain in its calculation, whereas the proportion of loss to gain measure differentiates countries experiencing deforestation or another loss dynamic without a corresponding forest recovery signal. The two ratio measures normalize the forest dynamic in order to directly compare national-scale change regardless of country size or absolute area of change dynamic. In fig. S1, countries that have lost forests without gain are high on the y axis (Paraguay, Mongolia, and Zambia). Countries with a large fraction of forest

area disturbed and/or reforested/afforested are high on the x axis (Swaziland, South Africa, and Uruguay). Thirty-one countries have an aggregate dynamic >1% per year, 11 have annual loss rates >1%, and 5 have annual gain rates of >1%. Figure S2 compares forest change dynamics disaggregated by ecozone (<http://foris.fao.org/static/data/fra2010/ecozones2010.jpg>).

Brazil is a global exception in terms of forest change, with a dramatic policy-driven reduction in Amazon Basin deforestation. Although Brazilian gross forest loss is the second highest globally, other countries, including Malaysia, Cambodia, Côte d'Ivoire, Tanzania, Argentina, and Paraguay, experienced a greater percentage of loss of forest cover. Given consensus on the value of natural forests to the Earth system, Brazil's policy intervention is an example of how awareness of forest valuation can reverse decades of previous widespread deforestation. International policy initiatives, such as the United Nations Framework Convention of Climate Change Reducing Emissions from Deforestation and forest Degradation (REDD) program (13), often lack the institutional investment and scientific capacity to begin implementation of a program that can make use of the global observational record; in other words, the policy is far ahead of operational capabilities (14). Brazil's use of Landsat data in documenting trends in deforestation was crucial to its policy formulation and implementation. To date, only Brazil produces and shares spatially explicit information on annual forest extent and change. The maps and statistics we present can be used as an initial reference for a number of countries lacking such data, as a spur to capacity building in the establishment of national-scale forest extent and change maps, and as a basis of comparison in evolving national monitoring methods.

Global-scale studies require systematic global image acquisitions available at low or no direct

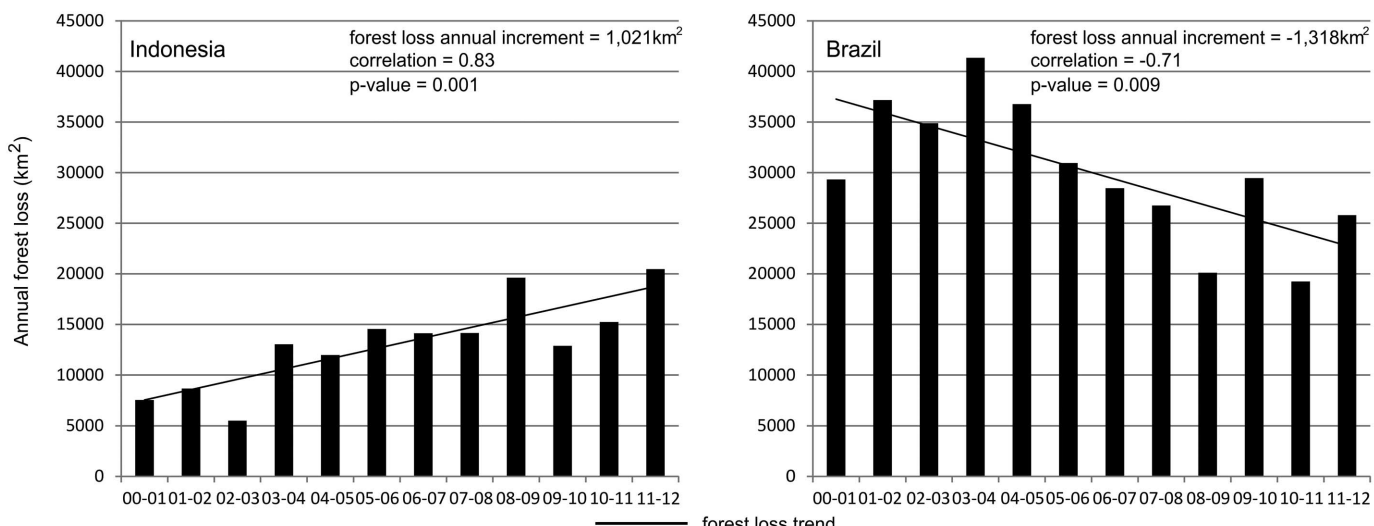


Fig. 3. Annual forest loss totals for Brazil and Indonesia from 2000 to 2012. The forest loss annual increment is the slope of the estimated trend line of change in annual forest loss.

cost and the preprocessing of geometric and radiometric corrections of satellite imagery, exemplified by the Landsat program. Given such progressive data policies and image processing capabilities, it is now possible to use advanced computing systems, such as the Google cloud, to efficiently process and characterize global-scale time-series data sets in quantifying land change. There are several satellite systems in place or planned for collecting data with similar capabilities to Landsat. Similar free and open data policies would enable greater use of these data for public good and foster greater transparency of the development, implementation, and reactions to policy initiatives that affect the world's forests.

The information content of the presented data sets, which are publicly available, provides a transparent, sound, and consistent basis on which to quantify critical environmental issues, including (i) the proximate causes of the mapped forest disturbances (15); (ii) the carbon stocks and associated emissions of disturbed forest areas (16–18); (iii) the rates of growth and associated carbon stock gains for both managed and unmanaged forests (19); (iv) the status of remaining intact natural forests of the world and threats to biodiversity (20, 21); (v) the effectiveness of existing protected-area networks (22); (vi) the economic drivers of natural forest conversion to more intensive land uses (23); (vii) the relationships between forest dynamics and social welfare, health,

and other relevant human dimensions data; (viii) forest dynamics associated with governance and policy actions—and many other regional-to-global-scale applications.

References and Notes

- J. A. Foley *et al.*, *Science* **309**, 570–574 (2005).
- M. C. Hansen, S. V. Stehman, P. V. Potapov, *Proc. Natl. Acad. Sci. U.S.A.* **107**, 8650–8655 (2010).
- Food and Agricultural Organization of the United Nations, *Global Forest Land-Use Change 1990–2005, FAO Forestry Paper No. 169* (Food and Agricultural Organization of the United Nations, Rome, 2012).
- M. Hansen, R. DeFries, *Ecosystems* **7**, 695–716 (2004).
- Instituto Nacional de Pesquisas Especiais, *Monitoring of the Brazilian Amazonian Forest by Satellite, 2000–2012* (Instituto Nacional de Pesquisas Especiais, San Jose dos Campos, Brazil, 2013).
- G. Sparovek, G. Berndes, A. G. O. P. Barreto, I. L. F. Klug, *Environ. Sci. Policy* **16**, 65–72 (2012).
- D. P. Edwards, W. F. Laurance, *Nature* **477**, 33 (2011).
- M. Drummond, T. Loveland, *Bioscience* **60**, 286–298 (2010).
- W. A. Kurz *et al.*, *Nature* **452**, 987–990 (2008).
- B. Gardiner *et al.*, *Destructive Storms in European Forests: Past and Forthcoming Impacts* (European Forest Institute, Freiburg, Germany, 2010).
- P. Potapov, M. Hansen, S. Stehman, T. Loveland, K. Pittman, *Remote Sens. Environ.* **112**, 3708–3719 (2008).
- A. Prishchepov, D. Muller, M. Dubinin, M. Baumann, V. Radloff, *Land Use Policy* **30**, 873–884 (2013).
- United Nations Framework Convention on Climate Change, *Reducing Emissions from Deforestation in Developing Countries: Approaches to Stimulate Action – Draft Conclusions Proposed by the President* (United Nations Framework Convention on Climate Change Secretariat, Bonn, Germany, 2005).
- R. Houghton *et al.*, *Carbon Manage.* **1**, 253–259.
- H. Geist, E. Lambin, *Bioscience* **52**, 143–150 (2002).
- S. S. Saatchi *et al.*, *Proc. Natl. Acad. Sci. U.S.A.* **108**, 9899–9904 (2011).
- A. Baccini *et al.*, *Nature Clim. Change* **2**, 182–185 (2012).
- N. L. Harris *et al.*, *Science* **336**, 1573–1576 (2012).
- R. Waterworth, G. Richards, C. Brack, D. Evans, *For. Ecol. Manage.* **238**, 231–243 (2007).
- P. Potapov *et al.*, *Ecol. Soc.* **13**, 51 (2008).
- T. M. Brooks *et al.*, *Science* **313**, 58–61 (2006).
- A. S. Rodrigues *et al.*, *Nature* **428**, 640–643 (2004).
- T. Rudel, *Rural Sociol.* **63**, 533–552 (1998).

Acknowledgments: Support for Landsat data analysis and characterization was provided by the Gordon and Betty Moore Foundation, the United States Geological Survey, and Google, Inc. GLAS data analysis was supported by the David and Lucile Packard Foundation. Development of all methods was supported by NASA through its Land Cover and Land Use Change, Terrestrial Ecology, Applied Sciences, and MEASUREs programs (grants NNN05ZDA001N, NNN07ZDA001N, NN12AB43G, NNX12AC78G, NNX08AP33A, and NNG06GD95G) and by the U.S. Agency for International Development through its CARPE program. Any use of trade, firm, or product names is for descriptive purposes only and does not imply endorsement by the U.S. government. Results are depicted and viewable online at full resolution: <http://earthinginepartners.appspot.com/science-2013-global-forest>.

Supplementary Materials

- www.sciencemag.org/content/342/6160/850/suppl/DC1
 Materials and Methods
 Supplementary Text
 Figs. S1 to S8
 Tables S1 to S5
 References (24–40)
 14 August 2013; accepted 15 October 2013
 10.1126/science.1244693

Changes in Cytoplasmic Volume Are Sufficient to Drive Spindle Scaling

James Hazel,¹ Kaspars Krutkramelis,² Paul Mooney,¹ Miroslav Tomschik,¹ Ken Gerow,³ John Oakey,² J. C. Gatlin^{1*}

The mitotic spindle must function in cell types that vary greatly in size, and its dimensions scale with the rapid, reductive cell divisions that accompany early stages of development. The mechanism responsible for this scaling is unclear, because uncoupling cell size from a developmental or cellular context has proven experimentally challenging. We combined microfluidic technology with *Xenopus* egg extracts to characterize spindle assembly within discrete, geometrically defined volumes of cytoplasm. Reductions in cytoplasmic volume, rather than developmental cues or changes in cell shape, were sufficient to recapitulate spindle scaling observed in *Xenopus* embryos. Thus, mechanisms extrinsic to the spindle, specifically a limiting pool of cytoplasmic component(s), play a major role in determining spindle size.

Organelles and other intracellular structures must scale with cell size in order to function properly. Maintenance of these dimensional relationships is challenged by the rapid and reductive cell divisions that characterize early embryogenesis in many organisms. The cellular machine that drives these divisions, the

mitotic spindle, functions to segregate chromosomes in cells that vary greatly in size while also adapting to rapid changes in cell size. The issue of scale is epitomized during *Xenopus* embryogenesis, where a rapid series of divisions reduces cell size 100-fold: from the 1.2-mm-diameter fertilized egg to ~12-μm-diameter cells in the adult frog (1). In large blastomeres, spindle length reaches an upper limit that is uncoupled from changes in cell size. However, as cell size decreases, a strong correlation emerges between spindle length and cell size (2). Although this scaling relationship has been characterized *in vivo* for several differ-

ent organisms, little is known about the direct regulation of spindle size by cell size or the underlying mechanism(s) (2–4). Spindle size may be directly dictated by the physical dimensions of a cell, perhaps through microtubule-mediated interaction with the cell cortex [i.e., boundary sensing (5–7)]. Alternatively, cell size could constrain spindle size by providing a fixed and finite cytoplasmic volume and, therefore, a limiting pool of resources such as cytoplasmic spindle assembly or length-determining components [i.e., component limitation (8, 9)]. Last, mechanisms intrinsic to the spindle could be actively tuned in response to systematic changes in cytoplasmic composition occurring during development [i.e., developmental cues (10, 11)].

To elucidate the responsible scaling mechanism(s), we developed a microfluidic-based platform to confine spindle assembly in geometrically defined volumes of *Xenopus* egg extract (12). Interphase extract containing *Xenopus* sperm nuclei was induced to enter mitosis and immediately pumped into a microfluidic droplet-generating device before nuclear envelope breakdown and the onset of spindle assembly. At the same time, a fluorinated oil/surfactant mixture was pumped into the device through a second inlet. These two discrete, immiscible phases merged at a T-shaped junction within the device to produce stable emulsions of extract droplets in a continuous oil phase (Fig. 1, A and C). Changing the T-junction channel dimensions and relative flow rates of the two phases

¹Department of Molecular Biology, University of Wyoming, Laramie, WY 82071, USA. ²Department of Chemical and Petroleum Engineering, University of Wyoming, Laramie, WY 82071, USA. ³Department of Statistics, University of Wyoming, Laramie, WY 82071, USA.

*Corresponding author. E-mail: jgatlin@uwyo.edu